Spin-trimer antiferromagnetism in $La_4Cu_3MoO_{12}$

Y. Qiu*
Department of Physics and Astronomy, Johns Hopkins University, Baltimore, Maryland 21218, USA

C. Broholm
Department of Physics and Astronomy, Johns Hopkins University, Baltimore, Maryland 21218, USA
and NIST Center for Neutron Research, National Institute of Standards and Technology, Gaithersburg, Maryland 20899, USA

S. Ishiwata, M. Azuma, and M. Takano
Institute for Chemical Research, Kyoto University, Uji, Kyoto-fu 611-0011, Japan

R. Bewley
ISIS Facility, Rutherford Appleton Laboratory, Chilton, Didcot OX11 0QX, United Kingdom

W. J. L. Buyers
National Research Council, Chalk River Laboratories, Chalk River, Ontario K0J 1J0, Canada
(Received 30 March 2005; published 30 June 2005)

$La_4Cu_3MoO_{12}$ is a cluster antiferromagnet where copper spin-1/2 trimers form a network of strongly coupled spin trimers. The magnetic properties of this material have been examined using magnetic neutron scattering. At low temperatures, excitations from the ground state are observed at 7.5(3) meV and 132.5(5) meV. An additional peak in the neutron scattering spectrum, which appears at 125.0(5) meV on heating, is ascribed to a transition between excited states. The wave vector and temperature dependence of the inelastic magnetic scattering cross section are consistent with intratrimer transitions. Magnetic neutron diffraction reveals antiferromagnetic order below $T_N=2.6$ K with a wave vector $(\frac{1}{2}00)$. The ordered magnetic structure is described as intertrimer order where spin correlations within trimers are controlled by the strong intratrimer interactions. Combining the information derived from elastic and inelastic magnetic neutron scattering with group theoretical analysis, a consistent set of intratrimer interactions and ordered magnetic structures is derived. The experiment provides a simple worked example of magnetism associated with interatomic composite degrees of freedom in the extreme quantum limit.

DOI: 10.1103/PhysRevB.71.214439 PACS number(s): 75.10.Jm, 75.25.+z

I. INTRODUCTION

Geometrically frustrated magnets are distinguished by an anomalous cooperative paramagnetic phase extending to temperatures well below characteristic microscopic energy scales.[1] Fluctuations in this phase are strong and nontrivial in that they satisfy certain local constraints. In some cases, further cooling fails to produce a phase transition and the low-temperature state is quantum disordered.[2,3] In other cases, however, thermal or quantum fluctuations, magnetoelastic coupling, impurities, or subleading exchange interactions yield a finite value of $\langle \mathbf{S} \rangle$ at sufficiently low temperatures.[4–7]

To advance the understanding of geometrically frustrated magnetism, we have explored spin correlations in $La_4Cu_3MoO_{12}$, a material which affords a spectacular example of geometrical frustration in the quantum limit. $La_4Cu_3MoO_{12}$ is a monoclinic ABO_3-type cuprate with space group $P112_1/m$ and B cations in 1:3 ratio.[8] Shown in Fig. 1, the Cu_3MoO_4 layers of the material are built from Cu_3O triangular clusters, which we shall denote trimers. Consideration of the crystal structure and the Goodenough rules[10] indicates that intratrimer exchange interactions are orders of magnitude stronger than intertrimer interactions. Magnetic susceptibility data[8,11] show two distinct linear regimes for $1/\chi(T)$ versus temperature. For $T>400$ K the Curie-Weiss fit yields $\mu_{eff}=1.81\mu_B$ and $\Theta_W=-558$ K, which is consistent with strong intratrimer interactions. For $T<250$ K the Curie constant decreases by a factor of 0.39 and the Weiss constant decreases to -16 K. This indicates a crossover to a cooperative paramagnetic phase where each trimer represents a composite spin-1/2 degree of freedom. The small Weiss temperature in this phase indicates weak antiferromagnetic (AFM) intertrimer interactions. At lower temperatures still, a maximum in $\chi(T)$ and a peak in the specific heat indicate an antiferromagnetic phase transition at $T_N=2.6$ K.[11]

In this paper, we present a comprehensive neutron scattering study of $La_4Cu_3MoO_{12}$. Polarized and unpolarized inelastic neutron scattering data provide evidence for magnetic excited states 7.5(3) meV and 132.5(5) meV above the ground state. A calculation based on a simple intratrimer Hamiltonian is presented to explain the energy levels, the wave-vector dependence, and the temperature dependence of the inelastic neutron scattering cross section. Using elastic neutron diffraction we also show that $La_4Cu_3MoO_{12}$ has long-range antiferromagnetic order at low temperatures. While a unique ordered structure cannot be identified directly from the diffraction data, analysis based on ordering of composite spin-1/2 degrees of freedom on neighboring tri-

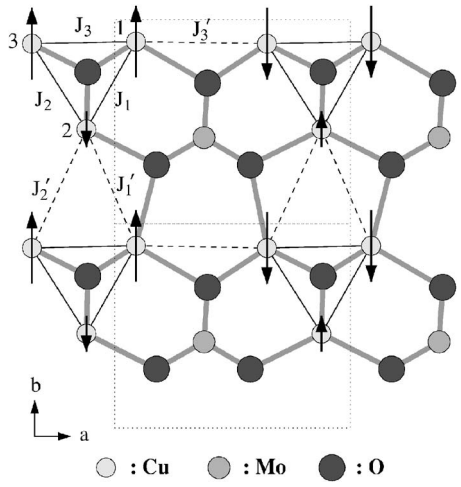

FIG. 1. Cu_3MoO_4 plane of $La_4Cu_3MoO_{12}$. Actual coordinates for copper atoms are given in the caption to Table II. The solid lines represent the triangle clusters. J_1, J_2, and J_3 are the intratriangle couplings; J's are the weak intertriangle couplings that are assumed to be antiferromagnetic and of similar magnitude as those in the mean-field analysis of Wessel and Haas (Ref. 9). The arrows illustrate one plane of the τ_2 magnetic structure with $\psi=0$ listed in Table II.

mers yields a consistent set of intratrimer exchange interactions and intertrimer spin configurations. The experiments and analysis provide a comprehensive understanding of geometrically frustrated quantum magnetism in a simple model system with important analogies to more complex systems.

II. EXPERIMENTAL RESULTS

A powder sample of $La_4Cu_3MoO_{12}$ was synthesized using a previously published method.[11] Rietveld analysis of powder neutron diffraction data confirmed a single-phase sample with space group $P112_1/m$ and lattice parameters $a=7.9119(5)$ Å, $b=6.8588(4)$ Å, $c=10.9713(3)$ Å, and $\gamma=90.008(9)°$ at 10 K. The elastic neutron scattering measurements were carried out on the BT2 thermal neutron triple-axis spectrometer at the NIST Center for Neutron Research. For that experiment we used a 30.2-g powder sample in a cylindrical container with a diameter of 1.6 cm. Pyrolytic graphite (PG) crystals set for (002) reflection were used to select 14.7-meV neutrons for diffraction. There was a PG filter in the incident beam to suppress higher-order contamination and collimations were 60′-40′-40′-200′ through the instrument from source to detector.

Inelastic neutron scattering measurements were performed on the HET direct geometry time-of-flight spectrometer at ISIS pulsed spallation neutron source. For that experiment we used an 80.2-g powder sample in a cylindrical container with a diameter of 3.1 cm. We used that instrument's "sloppy" chopper at frequencies of revolution 250 Hz and 400 Hz for incident energies of 40 meV and 160 meV, respectively.

Polarized inelastic neutron scattering measurements were performed on the C5 triple-axis spectrometer at the NRU

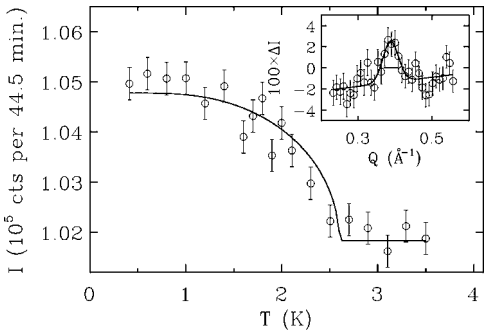

FIG. 2. Temperature dependence of the $(\frac{1}{2}00)$ magnetic Bragg peak intensity. The inset shows the wave-vector dependence of the difference between elastic magnetic neutron scattering at $T=0.4$ K and $T=10$ K. The energy resolution was 1.3 meV and the wave-vector resolution is indicated by the solid line in the inset.

reactor in Chalk River Laboratories in Canada. Magnetized Heusler crystals set for the polarizing (111) reflection were used as monochromator and analyzer with the latter fixed to reflect 14.6-meV neutrons. A cold sapphire filter was placed before the monochromator to eliminate high-energy neutrons. A PG filter was placed in the scattered beam to suppress order contamination at the analyzer. An energy-dependent correction was applied to the incident monitor count rate to account for incident beam $\lambda/2$ contamination. For this experiment we used a 120-g powder sample in a cylindrical container with a diameter of 2.5 cm. The collimation was 45′ in the incident and 80′ in the scattered beam. A Mezei flipper was placed in the scattered beam. The flipping ratio measured at 14.6 meV on a powder reflection was 24:1.

Absolute normalization turned out to be crucial to derive information about the magnetic structure. We used nuclear Bragg scattering to normalize the magnetic Bragg peak intensity.[7] The inelastic neutron scattering data were normalized by comparison to incoherent elastic count rates from a 20.14-g vanadium sample in the ISIS experiment. A correction for neutron absorption in $La_4Cu_3MoO_{12}$ was applied in this latter case.

A. Elastic neutron scattering

Figure 2 shows the temperature dependence of magnetic neutron diffraction at $Q=0.397$ Å^{-1}. The data are evidence for an antiferromagnetic phase transition at $T_N=2.6$ K $\ll\Theta_W$. The inset shows temperature difference data indicating that elastic scattering from the low-temperature spin structure is in the form of a well-defined Bragg peak. To within error the location of the peak is at $\frac{1}{2}a^*$, implying that the magnetic order doubles the unit cell in the **a** direction. After due consideration of the finite instrumental resolution (solid bar in the inset), we derive a lower limit of 100 Å for the magnetic correlation length.

B. Inelastic neutron scattering

Figure 3 shows the energy dependence of the scattering cross section at various temperatures. Because of the wide dynamic range, we show only the interesting magnetic parts

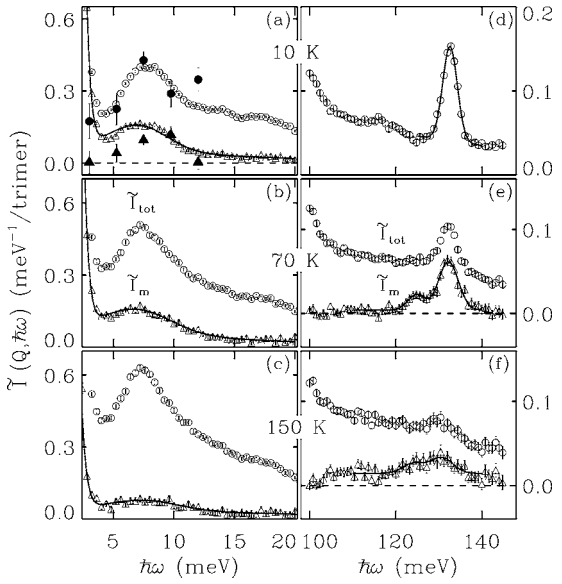

FIG. 3. $\hbar\omega$ dependence of the normalized Q-averaged neutron scattering intensity $\tilde{I}(Q,\hbar\omega)$ at various temeratures and in two different energy ranges. The open circles are raw experimental data. The open triangles are the phonon background subtracted data in (a)–(c) and the excess scattering above the background of the sloped Gaussian fit at 10 K for (e) and (f). The solid circles and solid triangles in (a) are total scattering and magnetic scattering intensities, respectively, from the polarized neutron measurement. A single scale factor was applied to the polarized data for best agreement with the unpolarized time-of-flight data.

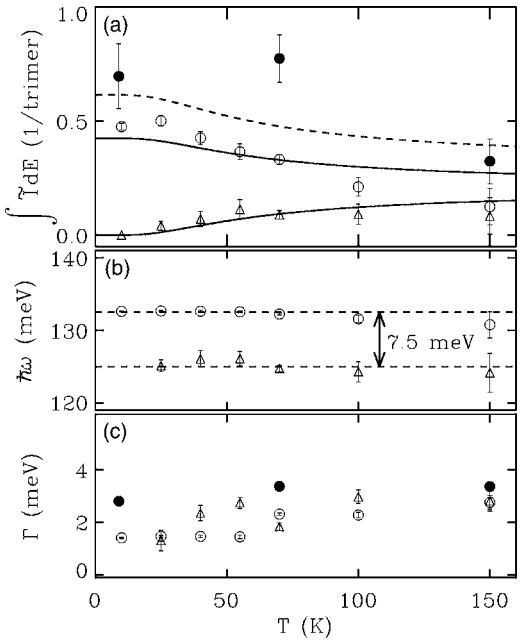

FIG. 4. Temperature dependence of parameters characterizing high- and low-energy magnetic excitations in $La_4Cu_3MoO_{12}$. Frame (a) shows the integrated intensities for the 132.5-meV (open circles), 125-meV (triangles), and 7.5-meV (solid circles) modes. Frame (b) shows the peak positions and frame (c) shows the intrinsic half width at half maximum relaxation rate for each mode. Lines in frame (a) were calculated from the trimer model.

of the spectrum, low energies on the left and higher energies on the right. The right panels clearly show an excitation at 132.5(5) meV. As temperature increases, the peak intensity at 132.5 meV decreases and a second peak emerges at $\hbar\omega = 125.0(5)$ meV. A likely explanation for the lower-energy peak is that it corresponds to a transition to the 132.5-meV state from an excited state at 132.5 meV$-$125 meV $\approx$7.5 meV, which is populated on heating. To explore this scenario, the left panels focus on the energy range around 7.5 meV. As is apparent from the increase of intensity with temperature, there is significant phonon scattering in the lower-energy range and this complicates the task of isolating a magnetic contribution to the scattering cross section. Since phonon scattering increases with temperature[12] while low-energy magnetic scattering generally decreases with temperature, we used high-temperature data (T=200 K) where magnetic scattering is negligible to determine the phonon density of states. At each temperature, the appropriate thermal factor was then applied to yield the phonon contribution to inelastic neutron scattering. The triangles in the left panels of Fig. 3 show the background subtracted data that indicate a residual peak in the excitation spectrum, which we tentatively associate with magnetic scattering.

To unambiguously verify the existence of a magnetic excitation at 7.5 meV, a polarized neutron scattering measurement was carried out at T=6 K and at a momentum transfer of 1.5 Å^{-1}. Only magnetic scattering can produce a difference between spin-flip scattering with guide fields at the sample position parallel and perpendicular to wave vector transfer.[13] Such difference data are shown as solid triangles in Fig. 3(a) and they provide immutable evidence for a magnetic excitation at 8(1) meV. Also shown is the sum of spin-flip and non-spin-flip scattering as solid circles. Twice the count rate with the analyzer turned through 4° was subtracted from the summed data and a single overall scale factor was applied to all the polarized data to facilitate comparison to the time-of-flight data (open circles). The excellent agreement between the two independent determinations of the magnetic contribution to inelastic scattering at 7.5 meV provides strong evidence for an intratrimer excited state at this energy.

From Gaussian fits to all inelastic data, we derived the temperature dependence of the integrated intensities, peak positions, and peak widths, which are reported in Fig. 4. For peak widths, the calculated energy resolution was subtracted in quadrature to produce values for the intrinsic half width at half maximum relaxation rate Γ or intertrimer bandwidth. The energy levels are temperature independent to within error as expected for intratrimer excitations. Γ is of order of the low-T Curie-Weiss temperature, which is consistent with intertrimer interactions being the main source of intratrimer level broadening. Transitions involving the excited-state doublet appear to have a greater relaxation rate than those involving other levels. Possible reasons for this include magnetoelastic effects and enhanced intertrimer coupling for trimers occupying the 7.5-meV excited state.

Figure 5 shows the wave-vector dependence of the energy-integrated intensity for the 7.5-meV and 132.5-meV modes. Kinematical limitations prevented measurement of

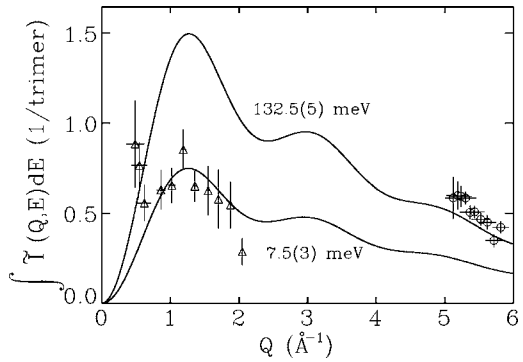

FIG. 5. Wave-vector dependence of the energy-integrated intensity for the 132.5-meV (circles) and 7.5-meV excitations (triangles) in $La_4Cu_3MoO_{12}$. Solid lines show the calculated Q dependence of the neutron scattering cross section from Eqs. (A6) and (A7) with no adjustable parameters.

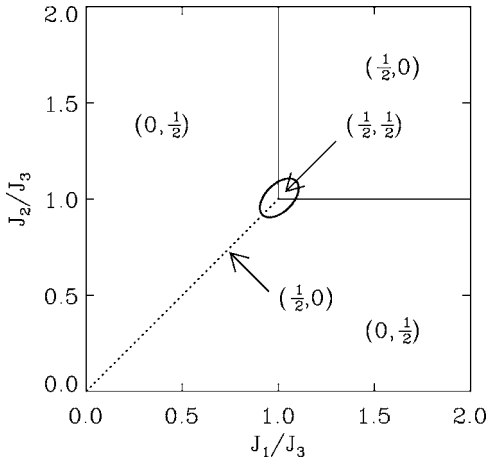

FIG. 6. Zero-temperature magnetic phase diagram of the AFM spin-1/2 trimer square lattice with a weak intertriangle coupling $J'=0.01J_3$. The excitation energies observed in the present experiment imply that the ratios of exchange constants lie on the ellipse shown in the center of the figure. The observation of $(\frac{1}{2}00)$ magnetic order also helps to constrain possible values of the exchange constants.

the high-energy excitations over a significant range of wave-vector transfer and at lower energies various types of nonmagnetic scattering give rise to large error bars especially at low values of Q. The result is that the Q dependence of the intensity for an individual mode does not provide a good measure of the trimer form factor. However, we shall see in the next section that the relative as well as the absolute intensities of the two modes are in good agreement with the scattering cross sections derived from a simple intratrimer exchange Hamiltonian (solid lines in Fig. 5).

III. ANALYSIS AND DISCUSSION

A. Energy level scheme for a spin-1/2 trimer

From the energy level scheme we can extract detailed information about intratrimer exchange interactions. The highest-energy state for a spin-1/2 trimer with antiferromagnetic Heisenberg interactions is a quartet with total spin 3/2. If the interactions within the trimer have the symmetry of an equilateral triangle, there is a fourfold-degenerate ground state composed of two degenerate Kramers doublets. For lower symmetry the degeneracy is lifted and there are two low-energy doublets. Spin-1/2 trimers in $La_4Cu_3MoO_{12}$ are made up from copper atoms in three different 2(e)-type sites with different positional parameters (see caption to Table II). While they approximate the symmetry of isosceles triangles with site 2 of Fig. 1 at the apex, the trimers have no exact symmetry elements. In the Appendix, we calculate the energy levels and scattering cross sections for a general spin-1/2 trimer with a model Hamiltonian of the form

$$H = J_1\mathbf{S}_1\cdot\mathbf{S}_2 + J_2\mathbf{S}_2\cdot\mathbf{S}_3 + J_3\mathbf{S}_3\cdot\mathbf{S}_1. \quad (1)$$

The splitting between the doublets is $E_{01}=\sqrt{J_1^2+J_2^2+J_3^2-J_1J_2-J_2J_3-J_3J_1}$ and the splitting between the ground-state doublet and the quartet is $E_{01}=\frac{1}{2}(J_1+J_2+J_3+E_{01})$. These energies can be associated, respectively, with the 7.5-meV and 132.5-meV transitions observed by inelastic neutron scattering. From this we can derive the average intratrimer exchange constant to be $\bar{J}=(2E_{02}-E_{01})/3=85.8$ meV. The splitting between doublets yields information about the ratios between intratrimer exchange constants. Ratios that are consistent with the 7.5-meV doublet-doublet transition lie on an ellipse in the J_1/J_3 versus J_2/J_3 plot shown in Fig. 6. The ellipse is centered at the equilateral point (1,1) and the major axis lies along the isosceles $J_1=J_2$ line. The half major axis is approximately $\sqrt{9E_{01}^2/(2E_{02}^2-2E_{01}E_{02})}=0.124$ and the half minor axis is approximately $\sqrt{3E_{01}^2/(2E_{02}^2-2E_{01}E_{02})}=0.071$. In the following, we shall label intratrimer interaction parameters that are consistent with the spectroscopic information by the counterclockwise azimuthal angle ψ on this ellipse with $\psi=0$ corresponding to $J_1=J_2$ and $\psi=n\pi$ describing isosceles triangles.

Wessel and Hass[9] studied the phase diagram for $La_4Cu_3MoO_{12}$ using a model Hamiltonian including the nearest-neighbor interactions within the a-b plane defined in Fig. 1. This study shows that different ratios of intratrimer interactions yield different in-plane wave vectors for long-range order. The wave vectors predicted in the limit of vanishing intertrimer interactions at $T=0$ are indicated on Fig. 6. Given that $T_N \ll \bar{J}$ this is the appropriate limit to consider. The study by Wang[14] using a different approach gives the same phase diagram. Taking into account this $T=0$ phase diagram leads to the conclusion that the azimuthal angle specifying intratrimer interaction asymmetry must satisfy $\psi=\pi$ or $-\pi/4<\psi<\pi/4$.

B. Q and T dependence of inelastic scattering

The spin-1/2 trimer model provides specific predictions for the Q and T dependence of inelastic scattering that are derived in the Appendix and compared to the experimental data in this section. In Fig. 5 the wave-vector dependences of the energy-integrated intensities for the two low-temperature modes are compared to the formulas of Eqs. (A6) and (A7).

TABLE I. The basis functions for irreducible representations of space group $P112_1/m$ with magnetic wave vector $(\frac{1}{2}00)$ and magnetic atoms on $2(e)$ sites.

Irreducible representation	$(x,y,\frac{1}{4})$	$(1-x,1-y,\frac{3}{4})$
τ_1	001	$00\bar{1}$
τ_2	100	100
	010	010
τ_3	100	$\bar{1}00$
	010	$0\bar{1}0$
τ_4	001	001

Considering that there are *no* adjustable parameters, the agreement between model and data is quite satisfactory. While the comparison does not provide information on intratrimer exchange, it supports the identification of a magnetic contribution to inelastic scattering at 7.5 meV, as the absolute cross section inferred from polarized and unpolarized magnetic neutron scattering is in perfect agreement with that predicted for the transition between the two doublets of the spin trimer.

The temperature dependence of the integrated intensities for the three inelastic peaks follows from Eq. (A6) to Eq. (A8). It depends only on the population of the intratrimer levels, which in turn only depends on E_{01} and E_{02}. The solid and dashed lines in Fig. 4(a) were calculated from these formulas using the experimental values for E_{01} and E_{02} and they are found to be in excellent agreement with the data.

C. Magnetic structure

Only the $(\frac{1}{2}00)$ magnetic Bragg peak could be detected in the present experiment. We obtained the absolute magnetic structure factor at $(\frac{1}{2}00)$ by comparison to the (230) nuclear Bragg peak. By combining this information with symmetry analysis and the spectroscopic information presented in Sec. III A, we can associate each of a few possible ordered structures with a specific set of intratrimer exchange constants.

The magnetic symmetry analysis is based on the assumption that any magnetic structure adopted through a second-order phase transition can be expanded in basis functions for a single irreducible representation of the magnetic space group.[15] Various programs are now available to carry out this type of analysis.[16] Table I lists the basis functions for the irreducible representations[17] contained in the reducible magnetic representation $La_4Cu_3MoO_{12}$. τ_1 and τ_4 describe uniaxial spin configurations with spins oriented along the **c** direction while τ_2 and τ_3 correspond to coplanar structures with spins in the **a**-**b** plane.

Because the three spins of a trimer are on three different $2(e)$-type sites, symmetry analysis does not link spin directions on these sites. However, a link is provided by the ground-state trimer wave function for a specific set of intratrimer exchange constants. The Appendix lists the eigenstates of the intratrimer spin Hamiltonian for arbitrary exchange interactions. Néel order corresponds to choosing a specific quantization axis on each spin trimer and alternating the Zeeman-split doublet occupation consistent with the $(\frac{1}{2}00)$ magnetic wave vector. Figure 7(a) shows the spin projection on the quantization axis, for each of the three atoms on a trimer as a function of the azimuthal angle ψ, which indexes intratrimer exchange constants that are consistent with our spectroscopic data. Given an irreducible magnetic representation and a value for ψ, the magnetic structure factor for the $(\frac{1}{2}00)$ Bragg peak can be calculated and compared to the measured absolute intensity.

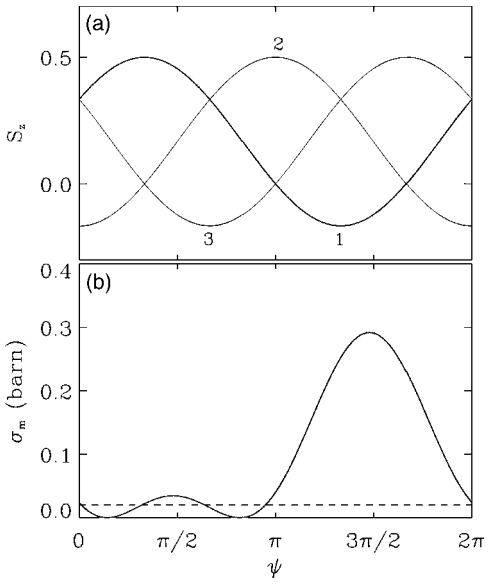

FIG. 7. (a) Expectation value for the magnetic moment along a small applied field and at $T=0$ for the three copper ions in a trimer as a function of index angle ψ. ψ is the azimuthal angle spanning intratrimer exchange interactions that are consistent with a 7.5-meV doublet-doublet transition (see Fig. 6). J_1/J_3 is equal to J_2/J_3 at $\psi=0$ and π. (b) Elastic magnetic neutron scattering cross section for the $(\frac{1}{2}00)$ Bragg peak per crystal unit cell calculated as a function of ψ when the spins are along the **c** direction and adopt the magnetic structure associated with the τ_4 irreducible representation. The dashed line shows the actual measured magnetic Bragg intensity.

Spin structures corresponding to irreducible representations τ_1 are inconsistent with the measured magnetic Bragg peak intensity for all values of ψ. For τ_4, Fig. 7(b) shows that the calculated intensity is consistent with the measured intensity for four different values of $\psi = (0.01(2), 0.32(4), 0.64(4), 0.94(2))\pi$. Of these solutions, only the first one is consistent with the stability analysis for the $(\frac{1}{2}00)$ structure[9] and it is also consistent with the approximately isosceles spin triangles.

Irreducible representations τ_2 and τ_3 describe spin configurations with spins in the **a**-**b** plane. Because of the constraint provided by the intratrimer ground-state wave function, only uniaxial spin configurations are possible. These are

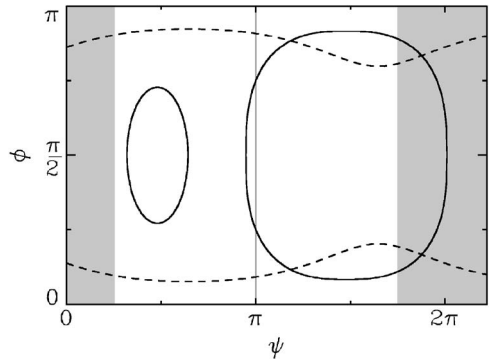

FIG. 8. Combination of index angle ψ and the spin orientation angle ϕ for magnetic structures with irreducible representation τ_2 (solid line) and τ_3 (dashed line) that yield a $\left(\frac{1}{2}00\right)$ magnetic Bragg intensity consistent with the experiment. Parameters in the hatched areas stabilize the $\left(\frac{1}{2}00\right)$ magnetic structure for weak intertrimer interactions (Ref. 9).

characterized by the angle ϕ between the spin-trimer quantization axis and the **a** direction. Figure 8 shows values for ψ and ϕ that are consistent with the measured $\left(\frac{1}{2}00\right)$ magnetic Bragg intensity. Also indicated as hatched areas are the values of ψ where the $\left(\frac{1}{2}00\right)$ structure is stable at low T with isotropic and uniform intertrimer interactions.[9]

As previously mentioned the trimers have an approximate mirror plane, and this leads to the expectation that $J_1 \approx J_2$. The eight spin structures and values of exchange constants that are consistent with this assumption are listed in Table II. Of these, the four structures with $\psi=0$ seem more likely because, as opposed to the $\psi=\pi$ structures, they have a finite range of stability in the J_1/J_3-J_2/J_3 plane (see Fig. 6).

IV. CONCLUSION

In summary we have presented neutron scattering data that provide detailed microscopic information about frustrated quantum magnetism in $La_4Cu_3MoO_{12}$. Neutron spectroscopy yields the average intratrimer exchange constant of 85.8 meV and narrows possible intratrimer exchange ratios to an elliptical trajectory in the J_1/J_3-J_2/J_3 plane. Neutron diffraction provides evidence for low-temperature intertrimer magnetic order that doubles the unit cell along the **a** direction. The $\left(\frac{1}{2}00\right)$ magnetic Bragg peak intensity and the approximate isosceles nature of the spin triangles narrow the possible exchange constants to $J_1=J_2=88$ meV and $J_3=81$ meV or $J_1=J_2=83$ meV and $J_3=91$ meV. A previously published mean-field analysis of magnetic order in $La_4Cu_3MoO_{12}$ indicates that the former combination of exchange constants is most likely. The corresponding ordered spin structures are uniaxial with two parallel spins at the base of the isosceles triangle $\left(\langle S_z\rangle=\frac{1}{3}\right)$ and an antiferromagnetically correlated spin of half the magnitude at the apex. The data are consistent with a spin direction either along **c**, **b**, or 25° away from **a** in the **a**-**b** plane. Unresolved by the present experiments is the magnetic stacking sequence along **c** for which there are two options for spins oriented in the **a**-**b** plane.

There is an instructive analogy between the frustrated cluster antiferromagnetism in $La_4Cu_3MoO_{12}$ and rare-earth magnets. In materials with Kramers rare-earth ions, intraatomic correlations establish effective spin-1/2 degrees of freedom, which subsequently develop long-range magnetic order due to interatomic exchange interactions.[18] Magnetic neutron scattering from such a system carries the rare-earth atomic form factor.[12] Magnetism in $La_4Cu_3MoO_{12}$ is also based on a composite spin-1/2 degree of freedom, only it is

TABLE II. Possible spin configurations corresponding to isosceles triangles with $J_1=J_2$. Coordinates for magnetic sites 1–6 are as follows: $\mathbf{r}_1=(x_1,y_1,0.25)$, $\mathbf{r}_4=(1-x_1,1-y_1,0.75)$, $\mathbf{r}_2=(x_2,y_2,0.25)$, $\mathbf{r}_5=(1-x_2,1-y_2,0.75)$, $\mathbf{r}_3=(x_3,y_3,0.25)$, and $\mathbf{r}_6=(1-x_3,1-y_3,0.75)$, where the positional parameters (x_i,y_i) are (1.0893, 0.8926), (0.8782, 0.4623), and (0.6465, 0.8816) for $i=1$, 2, and 3, respectively (Ref. 8).

	ψ	$J_{1,2}$ (meV)	J_3 (meV)	$\mathbf{S}_1$	$\mathbf{S}_2$	$\mathbf{S}_3$	$\mathbf{S}_4$	$\mathbf{S}_5$	$\mathbf{S}_6$
τ_2	0	88	81	$0\ \frac{1}{3}\ 0$	$0\ \frac{\bar{1}}{6}\ 0$	$0\ \frac{1}{3}\ 0$	$\mathbf{S}_1$	$\mathbf{S}_2$	$\mathbf{S}_3$
	π	83	91	000	$\frac{\sqrt{2}}{4}\ \frac{\sqrt{2}}{4}\ 0$	000	$\mathbf{S}_1$	$\mathbf{S}_2$	$\mathbf{S}_3$
	π	83	91	000	$\frac{\bar{\sqrt{2}}}{4}\ \frac{\sqrt{2}}{4}\ 0$	000	$\mathbf{S}_1$	$\mathbf{S}_2$	$\mathbf{S}_3$
τ_3	0	88	81	0.30 0.14 0	$\overline{0.15}\ \overline{0.07}\ 0$	0.30 0.14 0	$\overline{\mathbf{S}_1}$	$\overline{\mathbf{S}_2}$	$\overline{\mathbf{S}_3}$
	0	88	81	$\overline{0.30}$ 0.14 0	0.15 $\overline{0.07}$ 0	$0.\bar{3}0$ 0.14 0	$\overline{\mathbf{S}_1}$	$\overline{\mathbf{S}_2}$	$\overline{\mathbf{S}_3}$
	π	83	91	000	0.48 0.14 0	000	$\overline{\mathbf{S}_1}$	$\overline{\mathbf{S}_2}$	$\overline{\mathbf{S}_3}$
	π	83	91	000	$\overline{0.48}$ 0.14 0	000	$\overline{\mathbf{S}_1}$	$\overline{\mathbf{S}_2}$	$\overline{\mathbf{S}_3}$
τ_4	0	88	81	$00\ \frac{1}{3}$	$00\ \frac{\bar{1}}{6}$	$00\ \frac{1}{3}$	$\mathbf{S}_1$	$\mathbf{S}_2$	$\mathbf{S}_3$

TABLE III. Eigenvalues and eigenstates of the Hamiltonian H. The eigenstates listed in the table are not normalized. We use the following abbreviations: $J=\frac{1}{3}(J_1+J_2+J_3)$, $a=J_1J_2-J_3^2-J_3\Delta$, $b=J_1J_3-J_2^2-J_2\Delta$, $c=J_2J_3-J_1^2-J_1\Delta$, $A=J_1J_2-J_3^2+J_3\Delta$, $B=J_1J_3-J_2^2+J_2\Delta$, $C=J_2J_3-J_1^2+J_1\Delta$, and $\Delta=\sqrt{J_1^2+J_2^2+J_3^2-J_1J_2-J_2J_3-J_3J_1}$.

	E	$\|\phi\rangle$
0	$(-3J-2\Delta)/4$	$-\frac{a+c}{a}\alpha\beta\beta+\frac{c}{a}\beta\alpha\beta+\beta\beta\alpha$
		$-\frac{a+b}{a}\alpha\alpha\beta+\frac{b}{a}\alpha\beta\alpha+\beta\alpha\alpha$
1	$(-3J+2\Delta)/4$	$-\frac{A+C}{A}\alpha\beta\beta+\frac{C}{A}\beta\alpha\beta+\beta\beta\alpha$
		$-\frac{A+B}{A}\alpha\alpha\beta+\frac{B}{A}\alpha\beta\alpha+\beta\alpha\alpha$
2	$3J/4$	$\alpha\alpha\alpha$
		$\beta\beta\beta$
		$\alpha\beta\beta+\beta\alpha\beta+\beta\beta\alpha$
		$\alpha\alpha\beta+\alpha\beta\alpha+\beta\alpha\alpha$

spread over three atoms, it is established by interatomic exchange interactions, and it carries an oscillatory trimer "form factor." $La_4Cu_3MoO_{12}$ is thus a particularly simple example of a concept of increasing importance in quantum magnetism. End states and holes in Haldane spin chains,[19,20] impurity spins in high-temperature superconductors,[21] and spontaneously formed or structurally defined spin clusters in frustrated magnets[22,23] are all strongly correlated systems where suitably defined multiatom composite spin degrees of freedom provide an enormous simplification for understanding low-energy spin dynamics and the corresponding thermodynamic properties.

ACKNOWLEDGMENTS

Work at JHU was supported by the NSF through DMR-0074571 and by the US-Israel binational science foundation under Grant No. 2000-073.

APPENDIX: NEUTRON SCATTERING FROM A TRIMER

The Hamiltonian for a spin triangle with Heisenberg exchange interactions is

$$H=J_1\mathbf{S}_1\cdot\mathbf{S}_2+J_2\mathbf{S}_2\cdot\mathbf{S}_3+J_3\mathbf{S}_3\cdot\mathbf{S}_1. \tag{A1}$$

The eigenstates and eigenvalues are listed in Table III. Trimer calculations up to higher-order interactions can be found in Ref. 24. The differential magnetic neutron cross section for inelastic transitions $|S\rangle\rightarrow|S'\rangle$ is[12]

$$\frac{d^2\sigma}{d\Omega d\omega}=C_0\rho(S)\sum_{\alpha\beta}(\delta_{\alpha\beta}-\hat{Q}_\alpha\hat{Q}_\beta)\sum_{jj'}\exp[i\mathbf{Q}\cdot(\mathbf{R}_j-\mathbf{R}_{j'})]\sum_{MM'}\langle SM|\hat{S}_j^\alpha|S'M'\rangle\langle S'M'|\hat{S}_{j'}^\beta|SM\rangle\delta(\hbar\omega+E(S)-E(S')), \tag{A2}$$

where

$$C_0=N\left(\frac{\gamma e^2}{m_ec^2}\right)^2\frac{k'}{k}F^2(\mathbf{Q})\exp[-2W(\mathbf{Q})],$$

$$\rho(S)=Z^{-1}\exp\left[-\frac{E(S)}{k_BT}\right].$$

Also, $\mathbf{Q}=\mathbf{k}-\mathbf{k}'$ is the scattering wave vector, $F(\mathbf{Q})$ is the magnetic form factor,[25] and Z is the partition function. It can be shown that terms in the cross section with $\alpha\neq\beta$ vanish. After averaging over all directions for $\mathbf{Q}$ we obtain the following cross section for a powder sample:

$$\left(\frac{d^2\sigma}{d\Omega d\omega}\right)_{0\rightarrow1}=C_0\rho(0)\frac{2}{3}\left[1+\frac{\sin(QR_{12})}{QR_{12}}\frac{(J_1-J_2)(J_3-J_1)}{\Delta^2}+\frac{\sin(QR_{23})}{QR_{23}}\frac{(J_1-J_2)(J_2-J_3)}{\Delta^2}+\frac{\sin(QR_{13})}{QR_{13}}\frac{(J_1-J_3)(J_3-J2)}{\Delta^2}\right]\delta(\hbar\omega+E_0-E_1), \tag{A3}$$

$$\left(\frac{d^2\sigma}{d\Omega d\omega}\right)_{0\rightarrow2}=C_0\rho(0)\frac{2}{3}\left[2+\frac{\sin(QR_{12})}{QR_{12}}\left(\frac{-a(a+b)}{a^2+b^2+ab}+\frac{-bc}{b^2+c^2-bc}\right)+\frac{\sin(QR_{13})}{QR_{13}}\left(\frac{ab}{a^2+b^2+ab}+\frac{b(c-b)}{b^2+c^2-bc}\right)+\frac{\sin(QR_{23})}{QR_{23}}\left(\frac{-b(a+b)}{a^2+b^2+ab}+\frac{-c(c-b)}{b^2+c^2-bc}\right)\right]\delta(\hbar\omega+E_0-E_2), \tag{A4}$$

$$\left(\frac{d^2\sigma}{d\Omega d\omega}\right)_{1\rightarrow2}=C_0\rho(1)\frac{2}{3}\left[2+\frac{\sin(QR_{12})}{QR_{12}}\left(\frac{-A(A+B)}{A^2+B^2+AB}+\frac{-BC}{B^2+C^2-BC}\right)+\frac{\sin(QR_{13})}{QR_{13}}\left(\frac{AB}{A^2+B^2+AB}+\frac{B(C-B)}{B^2+C^2-BC}\right)+\frac{\sin(QR_{23})}{QR_{23}}\left(\frac{-B(A+B)}{A^2+B^2+AB}+\frac{-C(C-B)}{B^2+C^2-BC}\right)\right]\times\delta(\hbar\omega+E_1-E_2), \tag{A5}$$

where a, b, c, A, B, and C are defined in Table III. The spin triangles in $La_4Cu_3MoO_{12}$ are close to equilateral ($R_{12}=3.39$ Å, $R_{13}=3.50$ Å, $R_{23}=3.41$ Å), so we can replace the Cu-Cu distances by $R=\frac{1}{3}(R_{12}+R_{23}+R_{13})$:

$$\left(\frac{d^2\sigma}{d\Omega d\omega}\right)_{0\to 1} = C_0\rho(0)\frac{2}{3}\left[1-\frac{\sin(QR)}{QR}\right]\delta(\hbar\omega+E_0-E_1), \tag{A6}$$

$$\left(\frac{d^2\sigma}{d\Omega d\omega}\right)_{0\to 2} = C_0\rho(0)\frac{4}{3}\left[1-\frac{\sin(QR)}{QR}\right]\delta(\hbar\omega+E_0-E_2), \tag{A7}$$

$$\left(\frac{d^2\sigma}{d\Omega d\omega}\right)_{1\to 2} = C_0\rho(1)\frac{4}{3}\left[1-\frac{\sin(QR)}{QR}\right]\delta(\hbar\omega+E_1-E_2). \tag{A8}$$

As each level is degenerate there is also an elastic cross section associated with intralevel transitions. However, this is not relevant for the experiment and so will not be listed.

*Electronic address: qiuym@pha.jhu.edu

[1] A. P. Ramirez, in *Handbook on Magnetic Materials*, edited by K. J. H. Busch (Elsevier Science, Amsterdam, 2001), Vol. 13, p. 423.

[2] M. B. Stone, I. Zaliznyak, Daniel H. Reich, and C. Broholm, Phys. Rev. B **64**, 144405 (2001).

[3] M. B. Stone, Y. Chen, J. Rittner, H. Yardimci, D. H. Reich, C. Broholm, D. V. Ferraris, and T. Lectka, Phys. Rev. B **65**, 064423 (2002).

[4] S.-H. Lee, C. Broholm, T. H. Kim, W. Ratcliff II, and S-W. Cheong, Phys. Rev. Lett. **84**, 3718 (2000).

[5] S. H. Lee, C. Broholm, G. Aeppli, A. P. Ramirez, T. G. Perring, C. Carlile, M. Adams, and B. Hessen, Europhys. Lett. **35**, 127 (1996).

[6] J. S. Gardner, B. D. Gaulin, S.-H. Lee, C. Broholm, N. P. Raju, and J. E. Greedan, Phys. Rev. Lett. **83**, 211 (1999).

[7] S.-H. Lee, C. Broholm, M. F. Collins, L. Heller, A. P. Ramirez, Ch. Kloc, E. Bucher, R. W. Erwin, and N. Lacevic, Phys. Rev. B **56**, 8091 (1997).

[8] D. A. Vander Griend, S. Boudin, V. Caignaert, K. R. Poeppelmeier, Y. Wang, V. P. Dravid, M. Azuma, M. Takano, Z. Hu, and J. D. Jorgensen, J. Am. Chem. Soc. **121**, 4787 (1999).

[9] S. Wessel and S. Haas, Phys. Rev. B **63**, 140403(R) (2001).

[10] J. B. Goodenough, Prog. Solid State Chem. **5**, 145 (1972).

[11] M. Azuma, T. Odaka, M. Takano, D. A. Vander Griend, K. R. Poeppelmeier, Y. Narumi, K. Kindo, Y. Mizuno, and S. Maekawa, Phys. Rev. B **62**, R3588 (2000).

[12] S. W. Lovesey, *Theory of Thermal Neutron Scattering from Condensed Matter* (Clarendon Press, Oxford, 1984).

[13] R. M. Moon, T. Riste, and W. Koehler, Phys. Rev. **181**, 920 (1969).

[14] Han-Ting Wang, Phys. Rev. B **65**, 024426 (2001).

[15] Yu. A. Izyumov and V. E. Naish, J. Magn. Magn. Mater. **12**, 239 (1979); Yu. A. Izyumov, V. E. Naish, and R. P. Ozerov, *Neutron Diffraction of Magnetic Materials* (Consultants Bureau, New York, 1991).

[16] Software for magnetic symmetry analysis is available on the web at http://www.ftj.agh.edu.pl/zffs/sikora/ by W. Sikora and http://www.chem.ucl.ac.uk/people/wills/index.htm by A. S. Wills.

[17] Y. Qiu, Ph.D. thesis, Johns Hopkins University, 2002.

[18] J. Jensen and A. R. Mackintosh, *Rare Earth Magnetism* (Oxford University Press, New York, 1991).

[19] E. S. Sørensen and I. Affleck, Phys. Rev. B **51**, 16115 (1995).

[20] G. Xu, G. Aeppli, P. Bischer, C. Broholm, J. F. DiTusa, C. D. Frost, T. Ito, K. Oka, H. Takagi, and M. Treacy, Science **289**, 419 (2000).

[21] W. A. MacFarlane, J. Bobroff, H. Alloul, P. Mendels, N. Blanchard, G. Collin, and J. F. Marucco, Phys. Rev. Lett. **85**, 1108 (2000).

[22] R. Moessner and A. J. Berlinsky, Phys. Rev. Lett. **83**, 3293 (1999).

[23] P. G. Radaelli, Y. Horibe, M. J. Gutmann, H. Ishibashi, C. H. Chen, R. M. Ibberson, Y. Koyama, Y. S. Hor, V. Kiryukhin, and S.-W. Cheong, Nature (London) **416**, 155 (2002).

[24] A. Furrer, and H. U. Güdel, J. Magn. Magn. Mater. **14**, 256 (1979); U. Falk, A. Furrer, H. U. Güdel, and J. K. Kjems, Phys. Rev. Lett. **56**, 1956 (1986); U. Falk, A. Furrer, N. Furer, H. U. Güdel, and J. K. Kjems, Phys. Rev. B **35**, 4893 (1987).

[25] *International Tables for Crystallography*, edited by A. J. C. Wilson and E. Prince (Kluwer Academic, Boston, 1999).